The expanded immunoregulatory protease network in mosquitoes is governed by gene co-expression

Bianca Morejon[1] and Kristin Michel[1]*

[1]Division of Biology, Kansas State University; Manhattan, KS, 66502, USA

*Corresponding author. Email: kmichel@ksu.edu

Abstract:
Serine protease cascades regulate key innate immune responses. In mosquitoes, these cascades involve clip-domain serine proteases and their non-catalytic homologs (CLIPs), forming a complex network whose make-up and structural organization is not fully understood. This study assessed the impact of 85 CLIPs on humoral immunity in *Anopheles gambiae*. By coupling RNAi with assays measuring antimicrobial activity and melanization, we identified 27 CLIPs as immunoregulators that together form two distinct subnetworks. CLIPs regulating antimicrobial activity were found to control infection resistance, as knockdowns reduced bacterial load and improved survival. Furthermore, our analysis of CLIP gene expression unveiled a novel immunoregulatory mechanism reliant on protease baseline co-expression rather than infection-induced upregulation. These findings underscore that despite its complexity mosquito immune regulation may be targeted for malaria interventions.

Introduction:

The Afrotropical mosquito *Anopheles gambiae* is the primary vector responsible for the transmission of malaria parasites in most of sub-Saharan Africa. As malaria prevention relies on controlling mosquito populations, novel approaches hinge on a detailed molecular grasp of mosquito physiology, including innate immunity and its regulation (*1–3*). This knowledge is crucial for our fundamental understanding of vector competence in this most important human vector-borne disease (*4–6*).

Serine protease cascades play essential roles in a wide range of innate defense responses in animals, including blood clotting in mammals and horseshoe crab (*7*, *8*), and complement in mammals (*9*). In insects, these cascades consist of clip-serine proteases (cSPs) and their non-catalytic homologs (cSPHs), together known as CLIPs (*10*). Immune cascades involving CLIPs lead to the specific activation of prophenoloxidase (proPO), crucial for the melanization response (*11–14*). Furthermore, CLIP cascades can also result in the proteolytic activation of the cytokine Spätzle (SPZ), ultimately leading to the expression of Toll-regulated genes that include antimicrobial factors (*15–17*).

Genetic and biochemical studies in *An. gambiae* have identified multiple cSPs and cSPHs regulating proPO activity (*14*, *18–28*). These are organized into two functional modules: the cSP module, which comprises one or more interacting protease cascades, and the cSPH module,

which consists of a hierarchical arrangement of protease homologs (*21*). However, the identity and structural organization of these modules governing melanization are only partially defined, and the CLIP cascade leading to Toll pathway activation, and thus, antimicrobial activity, remains uncharacterized. To address these knowledge gaps, we developed a functional genetic screen to assess the impact of CLIPs on hemolymph antimicrobial activity and melanization in *An. gambiae* mosquitoes.

Results & Discussion:

An RNAi screen identifies 27 CLIPs as immunoregulators in *An. gambiae*.

The *An. gambiae* genome contains 110 CLIP genes, which are divided into 5 subfamilies (A-E), forming one of the largest protein families in mosquitoes (*29*). To specifically test the contribution of CLIPs to melanization and hemolymph antimicrobial activity, we coupled RNAi with the Melanization Associated Spot Assay (MelASA) and Zone of Inhibition (ZOI) assay in our screen strategy (Fig. 1A) (*23*, *30*). RNAi was employed to individually silence 85 out of the 110 CLIP genes across all subfamilies (table S1). Knockdown (kd) efficiencies were assessed via RT-qPCR 48 hours post dsRNA injections, with each individual CLIP gene demonstrating at least 50% silencing (fig. S1A and table S2). For the remaining 25 CLIPs (annotations based on (*29*)), we could either not design a dsRNA that had a single gene target, or we were unable to amplify a dsRNA construct due to lack of expression in adult mosquitoes.

Mosquitoes injected with dsRNA were tested for their humoral immune response to different doses of *Micrococcus luteus*. A high dose (OD_{600}= 5) induced a strong immune response, helping identify factors necessary for immune activation. Conversely, a low dose (OD_{600}= 0.1) initiated a minimal response, aiding in the identification of factors that inhibit immune activation. We validated this approach by silencing established positive and negative regulators of melanization and antimicrobial activity. Specifically, we targeted the proPO activation pathway components *CLIPB4* and *Serine protease inhibitor 2* (*SRPN2*), known to be required and inhibitory for melanization, respectively (*5*, *28*). Likewise, we silenced the Toll pathway components *REL1* and *CACTUS*, both known as necessary and inhibitory factors for antimicrobial activity, respectively (*30*).

Genes of interest were identified by setting thresholds relative to the median of three replicates (table S3-S6). For melanization candidates, the threshold was set to <-0.25 median log2 fold change (FC) of total spot area for positive regulators and to >0.25 for negative regulators. For antimicrobial activity candidates, the threshold was set as the median log2 FC of ZOI <-0.5 for positive regulators and >0.5 for negative regulators. Out of the 85 CLIP genes tested, 27 met the defined thresholds, with 20 genes regulating melanization (Fig. 1B, table S3 and S4), and eight genes regulating antimicrobial activity (Fig. 1B, table S5 and S6). The MelASA phenotypes were found within the CLIPA (8), B (6), and C (4) subfamilies, with no identified phenotypes in subfamilies D or E. Similarly, the ZOI phenotypes belonged mostly to the CLIPA (3), B (2) and C (2) subfamilies. However, unlike melanization, we identified one CLIP D as a regulator of antimicrobial activity. Notably, only *CLIPB10* kd met the established thresholds for both MelASA and ZOI phenotypes (Fig. 1B and C), indicating a minimal overlap between the cascades regulating melanization and antimicrobial activity.

To delve deeper into the potential common immune factors between melanization and antimicrobial activity, we expanded our screen to include components recognized as upstream

regulators of CLIP cascades. Specifically, we tested the impact of the *Thioester-containing protein 1* (*TEP1*), and the putative ortholog of the *Drosophila melanogaster* modular serine protease (hereby named '*MODSP1*') in these reactions. We observed that kds of *MODSP1* and *TEP1* met the threshold for MelASA positive regulator phenotypes, but not for ZOI phenotypes (Fig. 1B and C, table S3 and S5), indicating that these are not involved in the regulation of hemolymph antimicrobial activity.

Overall, these results suggest that the set of proteases regulating humoral immunity in *An. gambiae* is much larger than previously understood. The limited overlap among CLIPs and upstream immune factors in the regulation of melanization and antimicrobial activity supports the presence of largely distinct regulatory modules in these immune reactions.

An expanded repertoire of CLIPs regulates melanization.

To provide more robust evidence to support the obtained MelASA phenotypes, we performed two additional replicates testing genes whose kd exceeded the established thresholds for positive and negative regulation, respectively. Out of the 20 CLIPs that showed a MelASA phenotype, dsRNA injection of *CLIPA8*, *A28*, *SPCLIP1*, *CLIPB4*, *B8*, *B9*, *B10*, *B17*, *C3*, *C9*, *C12* and *C14* produced a significant reduction in melanotic excreta compared to the ds*GFP* injected mosquitoes (Fig. 2A and table S7). In contrast, kd of *CLIPA2*, *A5*, *A7*, *A13*, *A14* and *B12* significantly increased melanotic excreta amounts relative to the ds*GFP* controls (Fig. 2A and table S8).

Overall, our MelASA screen recapitulated the phenotypes of most of the previously characterized regulators of melanization. All but one (*C9*) were identified using other assays such as melanization of rodent malaria parasites upon *C-type lectin 4* (*CTL4*) kd (*18*, *20*, *25*), melanotic tumor formation after *SRPN2* depletion (*14*, *28*, *31*), and melanization of Sephadex beads (*32*). The phenotypes of previously identified cSPs from families B and C that act as proPO-activating proteases (PAPs) (*B4, B9, B10*) and those functioning upstream of these PAPs (B8, *B17*, C9) were all reproduced (*14*, *23*, *27*, *28*, *31*, *33*). For CLIPAs, most of the phenotypes of the previously characterized positive (*CLIPA8, A28, SPCLIP1)* and negative (*A2* and *A14*) regulators were also recapitulated (*18–20*, *25*). Nevertheless, we noticed some variability in the phenotypes of two CLIPAs. Specifically, we identified CLIPA5 and A7 as negative regulators of melanization, consistent with the findings of Volz et al. (*25*), which showed an increased melanization response to *Plasmodium berghei* ookinetes after ds*CLIPA5* and ds*A7* injection. The phenotypes we observed can be attributed to the specific silencing of *CLIPA5* and *A7* by their respective dsRNAs, with RT-qPCR analysis showing no evidence of cross-silencing between them or with *CLIPA14* (fig. S1B). However, recent publications have shown that these cSPHs are not involved in parasite melanization (*19*, *26*). Contrary to being a negative regulator, CLIPA7 seems to be essential for *Escherichia coli* melanization (*26*). Moreover, a deletion mutant of recombinant CLIPA7, as well as A6, and A12 have been shown to enhance proPO activation by CLIPB9 *in vitro* (*34*), especially when forming a high molecular weight complex with A4. Despite these findings, we did not observe a phenotype after silencing *CLIPA4*, *A6*, or *A12.* The evident variability in some CLIPA phenotypes may result from the same cSPH potentially performing distinct roles in signal propagation and amplification depending on whether it is situated upstream or downstream of the cSP-cSPH modules. Immunoregulatory cSPHs serve as efficient cofactors of PAPs to enhance PPO activation downstream of the cSPH module (*21*, *34*), and can exert their effects upstream of the cSP module by regulating the activation of key cSPs (*23*, *33*). Performing double kds between cSPHs, as well as co-silencing cSPs and cSPHs, will help identify or rule out redundancy in these roles and refine our

understanding of molecular interactions between CLIPs. Alternatively, the differences between the regulatory roles of some CLIPAs against *P. berghei*, Gram-positive and Gram-negative bacteria could stem from microbial class-specific functions linked to specific components of these protease cascades. Hence, it is plausible that certain phenotypes might not have been captured with our screen strategy.

Furthermore, with this assay we identified *CLIPB13* and *B20*, as well as *C3*, *C12*, *C14* as novel positive regulators, and *A5*, *A7*, *A13* and *B12* as novel negative regulators of melanization. Among these, *CLIPC12* and *C14* have been shown to group within one of the CLIPB clusters in phylogenetic analyses of the *An. gambiae* CLIP family (*29*), suggesting they might not belong to the CLIPC subfamily, and are instead CLIPBs. While *C14* is the closest paralog to *C12* (*29*), their expression levels were not altered by *C12* and *C14* kd, respectively, indicating that the obtained phenotypes as positive regulators are due to specific silencing by their corresponding dsRNAs (fig. S1C).

Based on these results, combined with the current understanding of the *An. gambiae* proPO activation cascades, we propose a model depicting the potential structural organization of these immunoregulatory cascades, and the interactions between their cSP and cSPH modules (Fig. 2B). Compared to other serine protease cascades with regulatory roles in animals (*7–9*), the *An. gambiae* melanization cascades feature an expanded number of proteases and form a complex regulatory network. Within this network, cSPs and cSPHs interact at multiple levels in positive and negative ways to regulate proPO activation. Future research should aim to refine the activation hierarchies within cSP and cSPH modules and explore the interactions within and between each module by identifying novel branching points and feedback loops.

A CLIP cascade regulates humoral antimicrobial activity in *An. gambiae.*

Similarly, we performed two additional replicates testing CLIPs whose kd exceeded the established thresholds for positive and negative regulation of antimicrobial activity. Silencing *CLIPA3*, *B10*, *B14*, *C2*, *C4* and *D3* significantly decreased the ZOI compared to the ds*GFP* controls (Fig. 3A and table S9). In contrast, dsRNA injection of *CLIPA4* and *A19* produced a significant increase in ZOI relative to the ds*GFP* controls (Fig. 3A and table S10). Overall, our results identified 6 positive and 2 negative regulators of antimicrobial activity. These findings represent the first report of CLIPs being involved in the regulation of antimicrobial activity in *An. gambiae* mosquitoes. Importantly, this also marks the first identification of a CLIPD as a regulator of humoral immunity in *An. gambiae*, and only the second such instance across all insects (*35*). Based on the current knowledge of the SPZ activation cascades in other insects, we propose for the first time a layout of the potential structural organization of these cascades in *An. gambiae* mosquitoes, and the interactions between their cSP and cSPH components (Fig. 3B). Remarkably, in this mosquito species, melanization and antimicrobial activity are regulated by mostly independent cascades, with CLIPB10 being the only component required for both immune responses. This is in clear contrast to other insects such as *D. melanogaster* and *Manduca sexta*, where some of the cascade members involved in Toll pathway activation also participate in the melanization response (*36*, *37*). These findings suggest that in mosquitoes, the regulation of these two immune responses has significantly diverged, and does not involve tightly integrated protease cascades.

CLIPs regulating insect antimicrobial activity are primarily recognized for cleaving SPZ proteins (*15*, *36*). As the SPZ ligand for TOLL in mosquitoes remains unidentified, we individually silenced the six annotated *SPZ* genes in the *An. gambiae* genome and assessed their impact on

179 antimicrobial activity. Notably, kd of *SPZ1* and *SPZ3* produced a significant reduction in ZOI
180 (fig. S2A and table S11), phenocopying the antimicrobial activity observed after silencing *REL1*
181 and *MYD88*, which are required intracellular components of the Toll signal transduction pathway
182 (*30*). Phenotypes were attributed to the individual silencing of *SPZ1* and *SPZ3*, as no evidence of
183 cross-silencing between them was detected (fig S2B). In addition, from the six annotated *SPZ*
184 genes, only *SPZ1* and *SPZ3* were expressed in adult female mosquitoes (table S12), as shown in
185 our previously published RNASeq data (*38*). Therefore, we have incorporated SPZ1 and SPZ3 as
186 putative TOLL ligands in our model of the SPZ activation cascades in *An. gambiae* (Fig. 3B).

187 **Regulators of humoral antimicrobial activity control resistance to bacterial infection.**

188 Organisms deploy two main strategies in their defense against pathogenic infection: resistance
189 and tolerance. In *D. melanogaster*, multiple studies have emphasized the involvement of diverse
190 antimicrobial factors in supporting these distinct defense mechanisms (*39–41*). Therefore, we
191 asked whether CLIPs that regulate antimicrobial activity play a role in conferring resistance to
192 infection caused by the pathogenic bacteria *Enterococcus faecalis*. To do so, we performed
193 microbial proliferation and survival assays using a GFP-expressing, tetracycline-resistant *E.*
194 *faecalis* strain (V583 (*42*)) that allowed us to specifically quantify changes in bacterial load 18 h
195 post-challenge.

196 We found a negative correlation between bacterial load and median survival after kd of positive
197 and negative regulators of antimicrobial activity (Fig. 3C). Silencing the negative regulators
198 *CLIPA4* and *A19* reduced bacterial load 18 h after challenge, and significantly increased median
199 survival (fig. S3, table S13 and S14) compared to ds*GFP* controls. In turn, kd of the positive
200 regulators *CLIPA3*, *C2*, *B10*, *B14*, and *D3* increased bacterial load 18 h after challenge. Among
201 these, *CLIPB10* and *B14* kds reduced median survival, while no difference was observed after
202 *CLIPA3, C2* and *D3* kds. Neither median survival nor bacterial load were impacted after kd of
203 the positive regulator *CLIPC4*. Interestingly, kd of *MODSP1* and *TEP1* also produced an
204 increase in bacterial load and reduction in median survival (Fig. 3C, table S13 and S14). These
205 results phenocopied those of *REL1* kd, despite MODSP1 and TEP1 not seeming to be directly
206 involved in the regulation of antimicrobial activity (Fig. 1C). Therefore, these two immune
207 factors may contribute to infection resistance through immune responses other than hemolymph
208 antimicrobial activity.

209 Overall, our results showed that higher bacterial load after silencing immunoregulatory CLIPs
210 was correlated with lower median survival, indicating that the regulators of humoral
211 antimicrobial activity contribute to resistance to infection. The control of resistance is not
212 exclusive to CLIPs regulating antimicrobial activity, as it has been shown that CLIPs and other
213 factors that regulate melanization (MODSP1) and opsonization (TEP1) also impact bacterial load
214 (*19*, *21*, *26*, *43*).

215 **Humoral immune regulators are characterized by co-expression but not response to**
216 **infection.**

217 Genes that encode CLIP family of proteases and their homologs are upregulated transcriptionally
218 after infection with either pathogenic and non-pathogenic bacteria; indeed, *CLIP*s are often
219 among those genes identified in RNASeq experiments that display a strong transcriptional
220 response to environmental stimuli (*44–46*). Using our previously published RNASeq data (*38*),
221 we therefore tested whether gene expression levels or changes upon infection were able to
222 discriminate between immunoregulatory and non-phenotypic CLIPs.

223 The normalized expression levels in unchallenged (UC) females were in average significantly
224 higher for CLIPs that regulate humoral immunity, as compared to those that did not (Fig. 4A,
225 table S15). We also observed that 15% of non-phenotypic CLIPs were not expressed in adult
226 females (table S15). When we removed all CLIP genes that were not expressed from the
227 analysis, expression levels of immunoregulatory CLIPs remained elevated as compared to those
228 without such function (fig. S4A and B). We obtained the same result when comparing expression
229 levels in mosquitoes challenged with pathogenic (*E. faecalis*) and non-pathogenic (*M. luteus*)
230 bacteria (fig. S4C-F). While 66% of CLIPs were positively regulated by infection (fig. S4G-H, J-
231 K), no difference was observed in average fold chance between immunoregulatory and non-
232 phenotypic CLIPs after challenge (Fig 4B, fig. S4L, table S15). This suggested that at least for
233 CLIPs, upregulation after infection is not a predictor for function in humoral immunity in *An.*
234 *gambiae*.

235 By examining node centrality measures in gene co-expression networks established in *An.*
236 *gambiae,* we recently identified CLIPB4 as a hub in a gene co-expression network, called
237 AgMelGCN (*28*). To determine whether high centrality is a general feature of immunoregulatory
238 CLIPs, we updated the existing network and built AgMelGCN2.0 using our recently published
239 pipeline (table S16) (*47*). We then reanalyzed node centralities for all CLIPs in the network
240 (table S17). Immunoregulatory CLIPs, on average, exhibited higher strength, eigenvector, and
241 closeness centrality in AgMelGCN2.0 compared to non-phenotypic CLIPs, while betweenness
242 remained similar (fig. S5A-D). These data showed that immunoregulatory CLIPs are co-
243 expressed with a higher number of members of the genes families that control melanization, and
244 suggested that immunoregulatory CLIPs are co-expressed on a transcriptional level. To test this
245 directly, we examined the distribution of immunoregulatory CLIPs in the network, and observed
246 them clustering significantly in community 2 (Fig. 4C, table S18). In contrast, non-phenotypic
247 CLIPs were enriched in community 4 (fig. S6A-C, table S18), demonstrating distinct co-
248 expression patterns and transcriptional regulation between immunoregulatory and non-
249 phenotypic CLIPs.

250 To determine whether this observed co-expression was an artifact of the gene selection used to
251 build AgMelGCN2.0, we performed the same analyses in the previously published
252 transcriptome-wide AgGCN1.0, built on the same 256 experimental conditions as
253 AgMelGCN2.0 (*47*). Overall, the CLIP gene family was nearly 10-fold enriched in community
254 7, as compared to all genes in the network (Fig. 4D, table S19). This enrichment was largely
255 driven by immunoregulatory and less so by non-phenotypic CLIPs (15-fold vs. 8-fold
256 enrichment in community 7, fig. S6D-F). Non-phenotypic CLIPs also clustered in community 2
257 (2-fold enrichment) (Fig. 4D). Together, these data confirmed that transcriptional regulation
258 differs between immunoregulatory and non-phenotypic CLIPs, and that immunoregulatory
259 CLIPs are globally co-expressed.

260 Our comprehensive genetic screen provides a foundation for future research into the intricate
261 molecular interactions and hierarchies within the *An. gambiae* immune system, revealing a
262 complex network of immunoregulatory proteases playing pivotal roles in defense mechanisms.
263 These findings have potential practical applications for developing new mosquito control
264 strategies, as a dysregulated immune response can reduce vectorial capacity by shortening the
265 lifespan of adult females (*5*, *48*). Immunoregulatory CLIPs could also be exploited to block
266 parasite transmission at both early (*14*, *18*, *20*, *25*) and late stages of *P. berghei* and *P.*
267 *falciparum* (*49*). Since these CLIPs regulate the melanization response, it would be interesting to
268 investigate whether CLIPs involved in antimicrobial activity can also be targeted, given their

269 crucial roles in mosquito fitness and infection resistance. By integrating our genetic approach
270 with gene expression and co-expression analyses, our findings underscore the complexity and
271 divergence in immune regulation mechanisms across insect species, highlighting the unique
272 evolutionary adaptations in mosquitoes.

273

274 **Materials and Methods**

275 Mosquito rearing

276 *Anopheles gambiae* (s.l) of the G3 strain (BEI Resources Accession # MRA-112) were reared as
277 described previously (*50*). Briefly, freshly hatched larvae were fed with a 2% (w/v) suspension
278 of baker's yeast (Fleischmann's Active Dry Yeast, AB Mauri, St. Louis, MO, USA) for 48 h,
279 followed by a slurry of 2% powdered fish food (TetraMin® Tropical Flakes, Tetra, Melle,
280 Germany) and baker's yeast at a 2:1 ratio. Upon emergence, adult mosquitoes were provided
281 with 8% fructose (Emprove Chemicals, Millipore Sigma, MO, USA) *ad libitum*. Female
282 mosquitoes were blood fed using commercial heparinized horse blood (PlasVacc, Templeton,
283 CA, USA) provided through an artificial membrane feeding system. All stages were housed in an
284 environmental chamber with conditions set at 27°C, 80% humidity, and a 12:12-h light:dark
285 cycle.

286

287 Double stranded RNA synthesis and *in vivo* gene silencing in female mosquitoes

288 DsRNA synthesis and adult female mosquito injections were performed as described previously
289 (*50*). PCR amplification of the genes of interest was performed using the T7-tagged primers
290 listed in table S1. Primer pair sequences for dsRNA templates were either obtained from former
291 publications or generated using the webtool for design of RNAi constructs E-RNAi (*51*). Target-
292 specific designs were obtained for 85 out of 110 CLIP genes annotated in the *Anopheles gambiae*
293 reference genome (PEST 4.11). In all experiments, 2 day old adult female mosquitoes were
294 injected intrathoracically with 69 nL of 3 ug/uL dsRNA solution using a nanoinjector (Nanoject
295 III, Drummond Scientific, Broomall, PA, USA). For kd control, mosquitoes were injected with
296 an equivalent amount of the non-targeting dsRNA of Green Fluorescent Protein (ds*GFP*).
297 Mosquitoes were allowed 48 h to recover before further manipulation.

298

299 Real Time-quantitative Polymerase Chain Reaction (RT-qPCR)

300 Efficiency of gene silencing was measured by RT-qPCR in mosquitoes collected 48 h after
301 dsRNA injection. Total RNA was extracted from 8 females per treatment and replicate using
302 TRIzol reagent (Invitrogen), and subsequently purified using an RNeasy mini kit (Qiagen,
303 Valencia, CA, USA). cDNA was synthesized using 100 ng of purified total RNA in a 20 µL
304 volume reaction with an iScript cDNA synthesis kit (Bio-Rad, Hercules, CA, USA), as described
305 in (*52*). RT-qPCR was performed using 2 µL of 1:5 diluted cDNA in a 20 µL volume reaction
306 with a PowerUp SYBR Green Master Mix (Thermo Fisher Scientific, Waltham, MA, USA), as
307 described previously (*30*). Primers used in RT-qPCR are listed in table S2. Relative gene
308 expression values were calculated using the method described in (*53*), taking into account the
309 primer efficiencies (table S2). Ribosomal protein S7 (*RpS7*) expression was used as reference
310 and ds*GFP* treatments as calibrator conditions. RT-qPCRs were performed in triplicate for each
311 sample and primer pair from three biological replicates.

312

313 RNAi screen

314 A functional genetic analysis pipeline was developed to assess the impact of CLIPs on humoral
315 immunity after bacterial challenge. The pipeline incorporated a Melanization Associated Spot

316 Assay (MelASA) and a Zone of Inhibition (ZOI) assay to test CLIPs contribution to melanization
317 and hemolymph antimicrobial activity in the same mosquitoes. After 48 h of dsRNA treatment,
318 50 female mosquitoes were challenged by injection with 50.6 nL of resuspended lyophilized
319 *Micrococcus luteus* (MilliporeSigma, Burlington, MA, USA). To prepare the inoculum,
320 lyophilized *M. luteus* was resuspended in 1x phosphate-buffered saline (PBS) and diluted to high
321 (OD_{600} = 5) and low (OD_{600} = 0.1) doses. To test for CLIPs and immune factors acting as
322 positive regulators of humoral immunity, dsRNA-injected mosquitoes were challenged with *M.*
323 *luteus* at the high dose, while negative regulators were tested by challenging with the low dose.
324 Sterile 1x PBS injections were used as negative controls. Following bacterial challenge, dsRNA-
325 injected mosquitoes were housed for 18 h in experimental cups containing P8-grade white filter
326 papers (Fisher Scientific, Pittsburgh, PA, USA) at the bottom. Batches of 7-10 candidate genes
327 were tested in independent groups using their own positive and negative controls. Three
328 independent biological replicates were performed using different mosquito generations. For
329 treatments where the median of the response variable surpassed the predefined phenotype cutoff
330 values for MelASA and ZOI assays, two extra biological replicates to enable statistical
331 evaluation of the screen results.
332
333 Melanization phenotype analysis
334 To assess CLIPs impact on melanization, MelASA was performed as described previously (*23*).
335 Briefly, the filter papers containing melanotic excreta were removed from the experimental cups
336 18 h post infection. Collected filter papers were imaged under white epi-illumination and without
337 filters in an Alpha Imager 2200 system (Alpha Innotech, San Leandro, CA, USA). Image
338 processing and total spot area measurements were performed as described by (*23*) with the
339 modifications described in (*28*). Positive controls for melanization regulation were established by
340 injecting mosquitoes with dsRNA targeting the prophenoloxidase-activating protease *CLIPB4* as
341 a positive regulator, and the serine-protease inhibitor *SRPN2* as a negative regulator (*23*, *28*, *33*).
342 Positive regulation phenotypes were defined by a log2 fold change (FC) of the median total spot
343 area <-0.25, and negative regulation phenotypes by a log2 FC of the median >0.25. Upon the
344 addition of two biological replicates for treatments that exceeded the phenotype cutoffs,
345 differences in total melanotic spot area were analyzed using One-Way ANOVA, followed by
346 Bonferroni's multiple comparisons post-test ($P < 0.05$).
347
348 Hemolymph antimicrobial activity phenotype analysis
349 To measure CLIPs impact on hemolymph antimicrobial activity, hemolymph collection and ZOI
350 assays were performed as described previously (*30*). Briefly, hemolymph from 40 dsRNA-
351 injected mosquitoes per treatment was collected and flash-frozen 18 h post infection. To prepare
352 ZOI plates, a 1:10 mixture of live *M. luteus* (ATCC, No. 4698) at an OD_{600} = 10 and 1% Luria-
353 Bertani (LB) agar was poured onto a 9 cm diameter Petri dish (Fisher Scientific, Waltham, MA,
354 USA). While the agar solidified, equidistant wells were created using a 3D-printed stencil with
355 metal pins, positioned 1.5 cm from the outer edge of the petri dish. After 4 minutes, the stencil
356 was removed, and each well was loaded with 1 μL of hemolymph per treatment. Plates were
357 incubated upside down for 16 h at 37 °C, and subsequently imaged under white epi-illumination
358 and without filters using the Azure 300 imaging system (Azure Biosystems Inc., Dublin, CA,
359 USA). Image processing and ZOI measurements were performed as described in (*30*). Positive
360 controls for antimicrobial activity regulation were included by injecting mosquitoes with dsRNA
361 targeting the NF-κB transcription factor *REL1* as a positive regulator, and the inhibitor of κB
362 *CACT* as a negative regulator. Positive regulation phenotypes were assigned if the median
363 log2FC in ZOI <-0.50, while negative regulation phenotypes were assigned for median log2FC

364 >0.50. After adding two replicates for treatments exceeding phenotype cutoffs, ZOI differences
365 were analyzed using One-Way ANOVA with Bonferroni's post-test ($P < 0.05$).
366
367 Bacterial Proliferation and Mosquito Survival Assays
368 To determine CLIPs impact on resistance to bacterial infections, microbial proliferation and
369 survival assays were adapted from the protocols developed by (*54*). Briefly, 35-50 dsRNA-
370 injected mosquitoes were injected intrathoracically with 50.6 nL of GFP-expressing,
371 tetracycline-resistant *Enterococcus faecalis* (strain V583, (*42*)). To prepare the bacterial
372 challenge, 2 mL of Todd-Hewitt broth were inoculated with a single colony of *E. faecalis*, then
373 incubated for 16 h at 37 °C. Cultures were centrifuged 20 mins at 2000 rpm, washed with 1 x
374 PBS, resuspended in 1 ml sterile 1x PBS and diluted to an OD_{600}= 0.08 (corresponding to an
375 average dose of 5.3 x 10^7 CFUs/mL).
376 Batches of 8 mosquitoes per treatment were ground in 400 µL Todd-Hewitt broth 18 h post-
377 challenge, then adjusted to a final volume of 1 mL with the same medium. To determine the
378 number of viable *E. faecalis* cells in whole mosquito homogenates, the track dilution bacteria
379 enumeration technique was used as described in (*55*). Homogenates were diluted 10^3-fold, and
380 20 µL samples were spotted in a row onto tetracycline-selective Todd Hewitt agar (15 µg/mL)
381 on 100×15 mm square plates (Fisher Scientific, Pittsburgh, PA, USA). Plates were tilted to a
382 45°–75° angle immediately after inoculation, allowing the diluted homogenate spots to migrate
383 in parallel tracks across the agar surface to the opposite side. Once the tracks were dried, usually
384 in less than a minute, the plates were incubated upside down for 16 h at 37 °C.
385 GFP-positive CFUs were scored under a fluorescence microscope (Leica EL6000, Leica
386 Microsystems, Wetzlar, Germany) for each treatment. Ds*GFP*-injected mosquitoes were used as
387 a negative control, while ds*REL1* and ds*CACT*-treated mosquitoes acted as positive controls for
388 positive and negative regulation of antimicrobial activity, respectively. Candidate genes were
389 tested in two independent groups using their own positive and negative controls. Potential
390 differences in CFU/mosquito from five independent biological replicates were analyzed using
391 One-way ANOVA followed by Bonferroni's multiple comparisons post-test ($P < 0.05$).
392 Survival of the remaining 35-40 mosquitoes per treatment was monitored daily until mortality
393 reached 100%. Survival curves were generated with the obtained data using the Kaplan–Meier
394 method, and statistically compared using the Log-rank (Mantel-Cox) test. Lethal time 50 (LT_{50},
395 the time point after challenge where 50 % of mosquitoes in a given treatment had died) was
396 statistically evaluated using One-way ANOVA followed by Bonferroni's multiple comparisons
397 post-test. Correlation between FC CFU/mosquito and FC LT_{50} was determined using Pearson
398 correlation.
399
400 CLIP gene expression analysis
401 Gene expression levels for the 85 CLIPs analyzed in the RNAi screen were derived from a prior
402 RNAseq study examining the transcriptomic response to various microbial systemic infections in
403 *An. gambiae* (*38*). Expression data normalized as log2 transcripts per million (TPM) was
404 extracted for unchallenged (UC) mosquitoes, as well as mosquitoes at 12 h post challenge with
405 either *M. luteus* or *E. faecalis.* Expression data for immunoregulatory vs. non-phenotypic CLIPs
406 exhibiting a normal distribution were analyzed with an unpaired two-tailed t-test, while those not
407 meeting the normal distribution criteria were assessed using a two-tailed Mann-Whitney test.
408
409 Gene-co expression analysis
410 To test for gene co-expression among CLIPs we rebuilt a gene co-expression network (GCN)
411 based on the z-score normalized gene co-expression matrix we had assembled previously (*28*)

using the GeCoNet-Tool (*56*) with a bin size of 10 and a 0.005 cutoff. The resulting undirected weighted network, which we named AgMelGCN2.0, contained 177 nodes and 958 edges. The edge list for this network can be accessed in table S16. We then used the GeCoNet-Tool to define communities based on the Louvain algorithm, the network core, and node centralities as described previously (*56*). Characteristics of each node in the AgMelGCN2.0 are summarized in table S17. Node centralities and community membership were used as measures to assess potential differences in gene co-expression between immunoregulatory vs. non-phenotypic CLIPs. Differences in node centralities in AgMelGCN2.0 were analyzed using a two-tailed Mann-Whitney test. Enrichment in community membership was assessed in the AgMelGCN2.0 as well as in the transcriptome-wide AgGCN1.0 network (*47*) using a hypergeometric test.

Statistical analyses

Statistical analyses were conducted using GraphPad Prism 10 Software (GraphPad Software, USA) unless specified otherwise. Normality of the data was assessed using Shapiro-Wilk tests. Parametric tests were applied to normally distributed data, and non-parametric tests were used for non-normally distributed data, as indicated for each assay. Survival curves were plotted, and log-rank pairwise comparisons were performed in R (version 4.2.0) using the packages *survival* (*57*), *survminer* (*58*), and *patchwork* (*59*). Node enrichments in network communities were assessed by calculating the *P* value for under- or over-enrichment based on the cumulative distribution function of the hypergeometric distribution in Excel according to (*60*).

Acknowledgments: We would like to thank all members of the Michel laboratory for mosquito rearing. We thank Dr. Lynn Hancock, University of Kansas for the kind gift of the *Enterococcus faecalis* strain. We gratefully acknowledge Dr. Ed Brokesh and the Intelligent Agar Solutions team (Ryan Cunningham, Seth Hoffman, Dugan Hult, Elizabeth Seidl) Kansas State University, Reno, for the design of the agar stencil. Figure panels 1A, 2B, and 3B were generated with Biorender.com. Finally, sincere thanks go to Dr. Michael R. Kanost, Kansas State University, for his continued support. Funding was provided by National Institutes of Health R01AI140760 (KM); USDA National Institute of Food and Agriculture Hatch project 1021223, and a Kansas State GRIP Seed grant (all to KM). This is contribution No. 24-249-J from the Kansas Agricultural Experiment Station. The contents of this article are solely the responsibility of the authors and do not necessarily represent the official views of the funding agencies.

Author contributions:

Conceptualization, Methodology, Investigation, Visualization, Writing (original draft, review, and editing): BM, KM; Funding acquisition, Project administration, Supervision: KM

Competing interests: Authors declare that they have no competing interests.

Data and materials availability: All data are available in the main text or the supplementary materials.

452 **References**

453 1. A. Ickowicz, S. D. Foster, G. R. Hosack, K. R. Hayes, Predicting the spread and persistence
454 of genetically modified dominant sterile male mosquitoes. *Parasit Vectors* **14**, 480 (2021).

455 2. T. Nolan, Control of malaria-transmitting mosquitoes using gene drives. *Philos Trans R Soc*
456 *Lond B Biol Sci* **376**, 20190803 (2021).

457 3. M. Sicard, M. Bonneau, M. Weill, Wolbachia prevalence, diversity, and ability to induce
458 cytoplasmic incompatibility in mosquitoes. *Curr Opin Insect Sci* **34**, 12–20 (2019).

459 4. S. Blandin, S.-H. Shiao, L. F. Moita, C. J. Janse, A. P. Waters, F. C. Kafatos, E. A.
460 Levashina, Complement-like protein TEP1 is a determinant of vectorial capacity in the
461 malaria vector Anopheles gambiae. *Cell* **116**, 661–670 (2004).

462 5. K. Michel, A. Budd, S. Pinto, T. J. Gibson, F. C. Kafatos, Anopheles gambiae SRPN2
463 facilitates midgut invasion by the malaria parasite Plasmodium berghei. *EMBO Rep* **6**, 891–
464 897 (2005).

465 6. E. L. G. Pryzdial, A. Leatherdale, E. M. Conway, Coagulation and complement: Key innate
466 defense participants in a seamless web. *Front Immunol* **13**, 918775 (2022).

467 7. L. Cerenius, K. Söderhäll, Coagulation in Invertebrates. *Journal of Innate Immunity* **3**, 3–8
468 (2010).

469 8. K. J. Kearney, J. Butler, O. M. Posada, C. Wilson, S. Heal, M. Ali, L. Hardy, J. Ahnström,
470 D. Gailani, R. Foster, E. Hethershaw, C. Longstaff, H. Philippou, Kallikrein directly
471 interacts with and activates Factor IX, resulting in thrombin generation and fibrin formation
472 independent of Factor XI. *Proceedings of the National Academy of Sciences* **118**,
473 e2014810118 (2021).

474 9. D. Ricklin, G. Hajishengallis, K. Yang, J. D. Lambris, Complement: a key system for
475 immune surveillance and homeostasis. *Nat Immunol* **11**, 785–797 (2010).

476 10. M. R. Kanost, H. Jiang, Clip-domain serine proteases as immune factors in insect
477 hemolymph. *Current Opinion in Insect Science* **11**, 47–55 (2015).

478 11. C. An, M. Zhang, Y. Chu, Z. Zhao, Serine protease MP2 activates prophenoloxidase in the
479 melanization immune response of Drosophila melanogaster. *PLoS One* **8**, e79533 (2013).

480 12. L. Cerenius, B. L. Lee, K. Söderhäll, The proPO-system: pros and cons for its role in
481 invertebrate immunity. *Trends Immunol* **29**, 263–271 (2008).

482 13. H. Kan, C.-H. Kim, H.-M. Kwon, J.-W. Park, K.-B. Roh, H. Lee, B.-J. Park, R. Zhang, J.
483 Zhang, K. Söderhäll, N.-C. Ha, B. L. Lee, Molecular control of phenoloxidase-induced
484 melanin synthesis in an insect. *J Biol Chem* **283**, 25316–25323 (2008).

485 14. X. Zhang, M. Li, L. El Moussawi, S. Saab, S. Zhang, M. A. Osta, K. Michel, CLIPB10 is a
486 Terminal Protease in the Regulatory Network That Controls Melanization in the African
487 Malaria Mosquito Anopheles gambiae. *Front Cell Infect Microbiol* **10**, 585986 (2020).

488 15. I.-H. Jang, N. Chosa, S.-H. Kim, H.-J. Nam, B. Lemaitre, M. Ochiai, Z. Kambris, S. Brun,
489 C. Hashimoto, M. Ashida, P. T. Brey, W.-J. Lee, A Spätzle-processing enzyme required for
490 toll signaling activation in Drosophila innate immunity. *Dev Cell* **10**, 45–55 (2006).

491 16. Z. Kambris, S. Brun, I.-H. Jang, H.-J. Nam, Y. Romeo, K. Takahashi, W.-J. Lee, R. Ueda,
492 B. Lemaitre, Drosophila immunity: a large-scale in vivo RNAi screen identifies five serine
493 proteases required for Toll activation. *Curr Biol* **16**, 808–813 (2006).

494 17. K.-B. Roh, C.-H. Kim, H. Lee, H.-M. Kwon, J.-W. Park, J.-H. Ryu, K. Kurokawa, N.-C.
495 Ha, W.-J. Lee, B. Lemaitre, K. Söderhäll, B.-L. Lee, Proteolytic cascade for the activation
496 of the insect toll pathway induced by the fungal cell wall component. *J Biol Chem* **284**,
497 19474–19481 (2009).

498 18. L. El Moussawi, J. Nakhleh, L. Kamareddine, M. A. Osta, The mosquito melanization
499 response requires hierarchical activation of non-catalytic clip domain serine protease
500 homologs. *PLoS Pathog* **15**, e1008194 (2019).

501 19. J. Nakhleh, G. K. Christophides, M. A. Osta, The serine protease homolog CLIPA14
502 modulates the intensity of the immune response in the mosquito Anopheles gambiae.
503 *Journal of Biological Chemistry* **292**, 18217–18226 (2017).

504 20. M. Povelones, L. Bhagavatula, H. Yassine, L. A. Tan, L. M. Upton, M. A. Osta, G. K.
505 Christophides, The CLIP-domain serine protease homolog SPCLIP1 regulates complement
506 recruitment to microbial surfaces in the malaria mosquito Anopheles gambiae. *PLoS*
507 *Pathog* **9**, e1003623 (2013).

508 21. S. A. Saab, X. Zhang, S. Zeineddine, B. Morejon, K. Michel, M. A. Osta, Insight into the
509 structural hierarchy of the protease cascade that regulates the mosquito melanization
510 response. *bioRxiv*, 2023.07.13.548954 (2023).

511 22. A. K. D. Schnitger, F. C. Kafatos, M. A. Osta, The Melanization Reaction Is Not Required
512 for Survival of Anopheles gambiae Mosquitoes after Bacterial Infections *. *Journal of*
513 *Biological Chemistry* **282**, 21884–21888 (2007).

514 23. G. L. Sousa, R. Bishnoi, R. H. G. Baxter, M. Povelones, The CLIP-domain serine protease
515 CLIPC9 regulates melanization downstream of SPCLIP1, CLIPA8, and CLIPA28 in the
516 malaria vector Anopheles gambiae. *PLOS Pathogens* **16**, e1008985 (2020).

517 24. J. Volz, M. A. Osta, F. C. Kafatos, H.-M. Müller, The Roles of Two Clip Domain Serine
518 Proteases in Innate Immune Responses of the Malaria Vector Anopheles gambiae. *Journal*
519 *of Biological Chemistry* **280**, 40161–40168 (2005).

520 25. J. Volz, H.-M. Muller, A. Zdanowicz, F. C. Kafatos, M. A. Osta, A genetic module
521 regulates the melanization response of Anopheles to Plasmodium. *Cell Microbiol* **8**, 1392–
522 1405 (2006).

523 26. R. Zakhia, M. A. Osta, CLIPA7 Exhibits Pleiotropic Roles in the Anopheles gambiae
524 Immune Response. *JIN* **15**, 317–332 (2023).

525 27. X. Zhang, C. An, K. Sprigg, K. Michel, CLIPB8 is part of the prophenoloxidase activation
526 system in Anopheles gambiae mosquitoes. *Insect Biochem Mol Biol* **71**, 106–115 (2016).

527 28. X. Zhang, S. Zhang, J. Kuang, K. A. Sellens, B. Morejon, S. A. Saab, M. Li, E. C. Metto,
528 C. An, C. T. Culbertson, M. A. Osta, C. Scoglio, K. Michel, CLIPB4 Is a Central Node in
529 the Protease Network that Regulates Humoral Immunity in Anopheles gambiae
530 Mosquitoes. *J Innate Immun* **15**, 680–696 (2023).

531 29. X. Cao, M. Gulati, H. Jiang, Serine protease-related proteins in the malaria mosquito,
532 Anopheles gambiae. *Insect Biochem Mol Biol* **88**, 48–62 (2017).

533 30. B. Morejon, K. Michel, A zone-of-inhibition assay to screen for humoral antimicrobial
534 activity in mosquito hemolymph. *Front. Cell. Infect. Microbiol.* **13**, 891577 (2023).

535 31. C. An, A. Budd, M. R. Kanost, K. Michel, Characterization of a regulatory unit that
536 controls melanization and affects longevity of mosquitoes. *Cell. Mol. Life Sci.* **68**, 1929–
537 1939 (2011).

538 32. S. M. Paskewitz, O. Andreev, L. Shi, Gene silencing of serine proteases affects
539 melanization of Sephadex beads in *Anopheles gambiae*. *Insect Biochemistry and Molecular*
540 *Biology* **36**, 701–711 (2006).

541 33. S. A. Saab, X. Zhang, S. Zeineddine, B. Morejon, K. Michel, M. A. Osta, Insight into the
542 structural hierarchy of the protease cascade that regulates the mosquito melanization
543 response. *Microbes and Infection* **26**, 105245 (2024).

544 34. Q. Jin, Y. Wang, Y. Hu, Y. He, C. Xiong, H. Jiang, Serine protease homolog pairs
545 CLIPA4-A6, A4-A7Δ, and A4-A12 act as cofactors for proteolytic activation of
546 prophenoloxidase-2 and -7 in Anopheles gambiae. *Insect Biochem Mol Biol* **164**, 104048
547 (2024).

548 35. X. Cao, H. Jiang, Building a platform for predicting functions of serine protease-related
549 proteins in Drosophila melanogaster and other insects. *Insect Biochemistry and Molecular*
550 *Biology* **103**, 53–69 (2018).

551 36. C. An, J. Ishibashi, E. J. Ragan, H. Jiang, M. R. Kanost, Functions of Manduca sexta
552 Hemolymph Proteinases HP6 and HP8 in Two Innate Immune Pathways. *J Biol Chem* **284**,
553 19716–19726 (2009).

554 37. T. Shan, Y. Wang, K. Bhattarai, H. Jiang, An evolutionarily conserved serine protease
555 network mediates melanization and Toll activation in Drosophila. *Science Advances* **9**,
556 eadk2756 (2023).

557 38. B. Hixson, L. Huot, B. Morejon, X. Yang, P. Nagy, K. Michel, N. Buchon, The
558 transcriptional response in mosquitoes distinguishes between fungi and bacteria but not
559 Gram types. *BMC Genomics* **25**, 353 (2024).

560 39. J. Huang, Y. Lou, J. Liu, P. Bulet, C. Cai, K. Ma, R. Jiao, J. A. Hoffmann, S. Liégeois, Z.
561 Li, D. Ferrandon, A Toll pathway effector protects Drosophila specifically from distinct

562 toxins secreted by a fungus or a bacterium. *Proc Natl Acad Sci U S A* **120**, e2205140120
563 (2023).

564 40. B. P. Lazzaro, T. B. Sackton, A. G. Clark, Genetic Variation in Drosophila melanogaster
565 Resistance to Infection: A Comparison Across Bacteria. *Genetics* **174**, 1539–1554 (2006).

566 41. K. Troha, J. H. Im, J. Revah, B. P. Lazzaro, N. Buchon, Comparative transcriptomics
567 reveals CrebA as a novel regulator of infection tolerance in D. melanogaster. *PLOS*
568 *Pathogens* **14**, e1006847 (2018).

569 42. D. F. Sahm, J. Kissinger, M. S. Gilmore, P. R. Murray, R. Mulder, J. Solliday, B. Clarke, In
570 vitro susceptibility studies of vancomycin-resistant Enterococcus faecalis. *Antimicrobial*
571 *Agents and Chemotherapy* **33**, 1588–1591 (1989).

572 43. A. S. Dekmak, X. Yang, H. Zu Dohna, N. Buchon, M. A. Osta, The Route of Infection
573 Influences the Contribution of Key Immunity Genes to Antibacterial Defense in Anopheles
574 gambiae. *J Innate Immun* **13**, 107–126 (2021).

575 44. M. Bonizzoni, W. A. Dunn, C. L. Campbell, K. E. Olson, M. T. Dimon, O. Marinotti, A. A.
576 James, RNA-seq analyses of blood-induced changes in gene expression in the mosquito
577 vector species, Aedes aegypti. *BMC Genomics* **12**, 82 (2011).

578 45. K. Chen, T. Tang, Q. Song, Z. Wang, K. He, X. Liu, J. Song, L. Wang, Y. Yang, C. Feng,
579 Transcription Analysis of the Stress and Immune Response Genes to Temperature Stress in
580 Ostrinia furnacalis. *Front. Physiol.* **10** (2019).

581 46. Z. Luo, Y. Yu, Q. Zhang, Z. Bao, J. Xiang, F. Li, Comparative Transcriptome Analysis
582 Reveals the Adaptation Mechanism to High Salinity in Litopenaeus vannamei. *Front. Mar.*
583 *Sci.* **9** (2022).

584 47. J. Kuang, N. Buchon, K. Michel, C. Scoglio, A global Anopheles gambiae gene co-
585 expression network constructed from hundreds of experimental conditions with missing
586 values. *BMC Bioinformatics* **23**, 170 (2022).

587 48. H. Yassine, L. Kamareddine, S. Chamat, G. K. Christophides, M. A. Osta, A Serine
588 Protease Homolog Negatively Regulates TEP1 Consumption in Systemic Infections of the
589 Malaria Vector Anopheles gambiae. *Journal of Innate Immunity* **6**, 806–818 (2014).

590 49. S. Zeineddine, S. Jaber, S. A. Saab, J. Nakhleh, G. Dimopoulos, M. A. Osta, Late
591 sporogonic stages of Plasmodium parasites are susceptible to the melanization response in
592 Anopheles gambiae mosquitoes. bioRxiv [Preprint] (2024).
593 https://doi.org/10.1101/2024.05.31.596773.

594 50. C. An, A. Budd, M. R. Kanost, K. Michel, Characterization of a regulatory unit that
595 controls melanization and affects longevity of mosquitoes. *Cell Mol Life Sci.* **68**, 1929–
596 1939 (2011).

597 51. T. Horn, M. Boutros, E-RNAi: a web application for the multi-species design of RNAi
598 reagents—2010 update. *Nucleic Acids Res* **38**, W332–W339 (2010).

599 52. V. L. Rhodes, M. B. Thomas, K. Michel, The interplay between dose and immune system
600 activation determines fungal infection outcome in the African malaria mosquito, Anopheles
601 gambiae. *Developmental & Comparative Immunology* **85**, 125–133 (2018).

602 53. M. W. Pfaffl, A new mathematical model for relative quantification in real-time RT-PCR.
603 *Nucleic Acids Research* **29**, 45e–445 (2001).

604 54. L. El Moussawi, J. Nakhleh, L. Kamareddine, M. A. Osta, The mosquito melanization
605 response requires hierarchical activation of non-catalytic clip domain serine protease
606 homologs. *PLoS Pathog* **15**, e1008194 (2019).

607 55. B. D. Jett, K. L. Hatter, M. M. Huycke, M. S. Gilmore, Simplified agar plate method for
608 quantifying viable bacteria. *Biotechniques* **23**, 648–650 (1997).

609 56. J. Kuang, K. Michel, C. Scoglio, GeCoNet-Tool: a software package for gene co-expression
610 network construction and analysis. *BMC Bioinformatics* **24**, 281 (2023).

611 57. T. M. Therneau, T. L. (original S.->R port and R. maintainer until 2009), A. Elizabeth, C.
612 Cynthia, survival: Survival Analysis, version 3.5-7 (2023);
613 https://lib.stat.cmu.edu/R/CRAN/web/packages/survival/index.html.

614 58. A. Kassambara, M. Kosinski, P. Biecek, S. Fabian, survminer: Drawing Survival Curves
615 using "ggplot2," version 0.4.9 (2021);
616 https://lib.stat.cmu.edu/R/CRAN/web/packages/survminer/index.html.

617 59. T. L. Pedersen, patchwork: The Composer of Plots, version 1.2.0 (2024);
618 https://lib.stat.cmu.edu/R/CRAN/web/packages/patchwork/index.html.

619 60. Hypergeometric p-value calculator.
620 https://systems.crump.ucla.edu/hypergeometric/index.php.

621

Figures

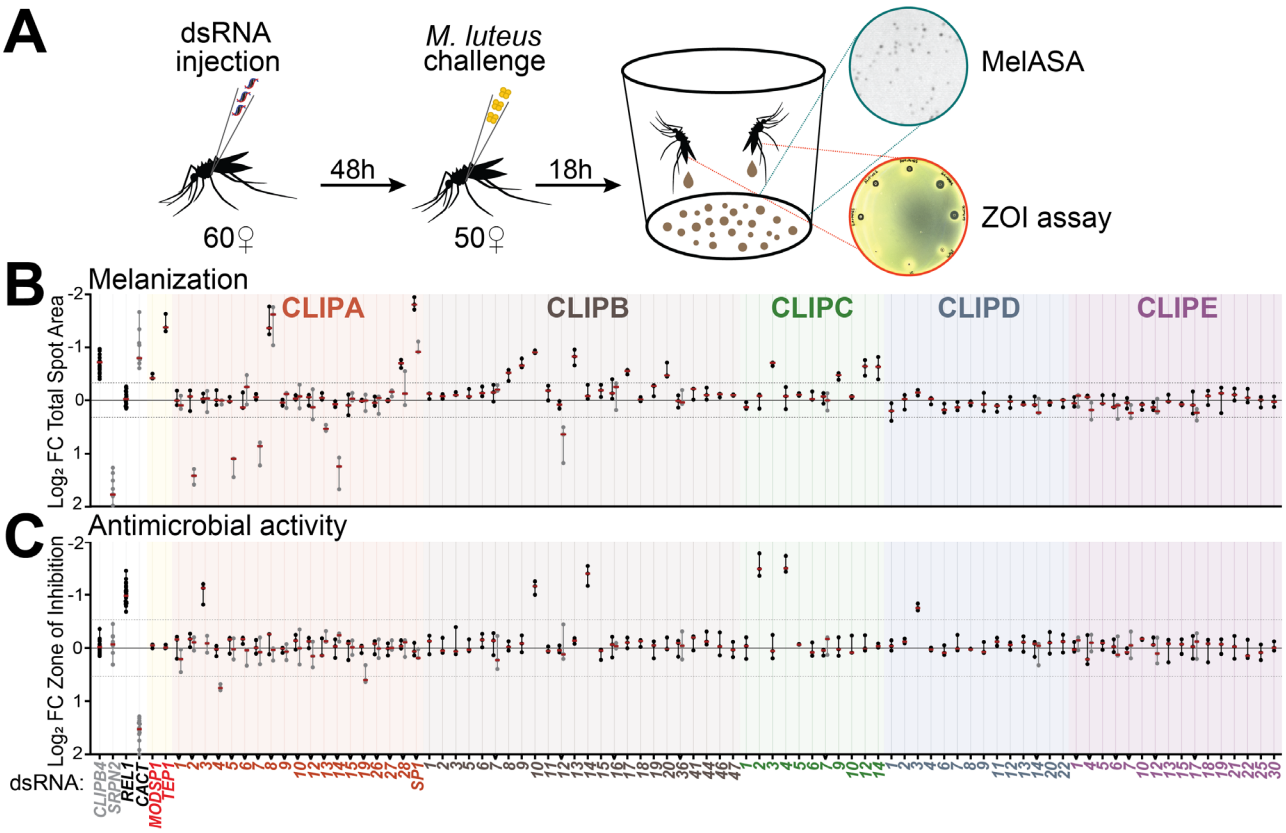

Fig. 1. CLIPs act as positive and negative regulators of melanization and antimicrobial activity. (**A**) Schematic of screen strategy. Batches of 60 female mosquitoes were injected with dsRNA to individually silence 85 CLIP genes. DsRNA injected mosquitoes were challenged with 50.6 nL of resuspended lyophilized *M. luteus* at $OD_{600} = 5$ and 0.1 for putative positive and negative regulators, respectively. The MelASA and ZOI assays were performed 18 h after challenge using the same mosquitoes. (**B**) MelASA RNAi screen. Data shown as log2 fold change (FC) Total spot area relative to ds*GFP* injected mosquitoes challenged with lyophilized *M. luteus* suspension (n=50). *CLIPB4* and *SRPN2* kds were used as positive controls for positive and negative regulators, respectively. (**C**) ZOI RNAi screen. Data shown as log2 FC ZOI relative to ds*GFP* injected mosquitoes challenged with lyophilized *M. luteus* suspension (n=40). *REL1* and *CACT* kds were used as positive controls for positive and negative regulators, respectively. Batches of 7-10 candidate genes were tested in independent groups using their own positive and negative controls. Red line and error bars represent median ± interquartile range from three biological replicates.

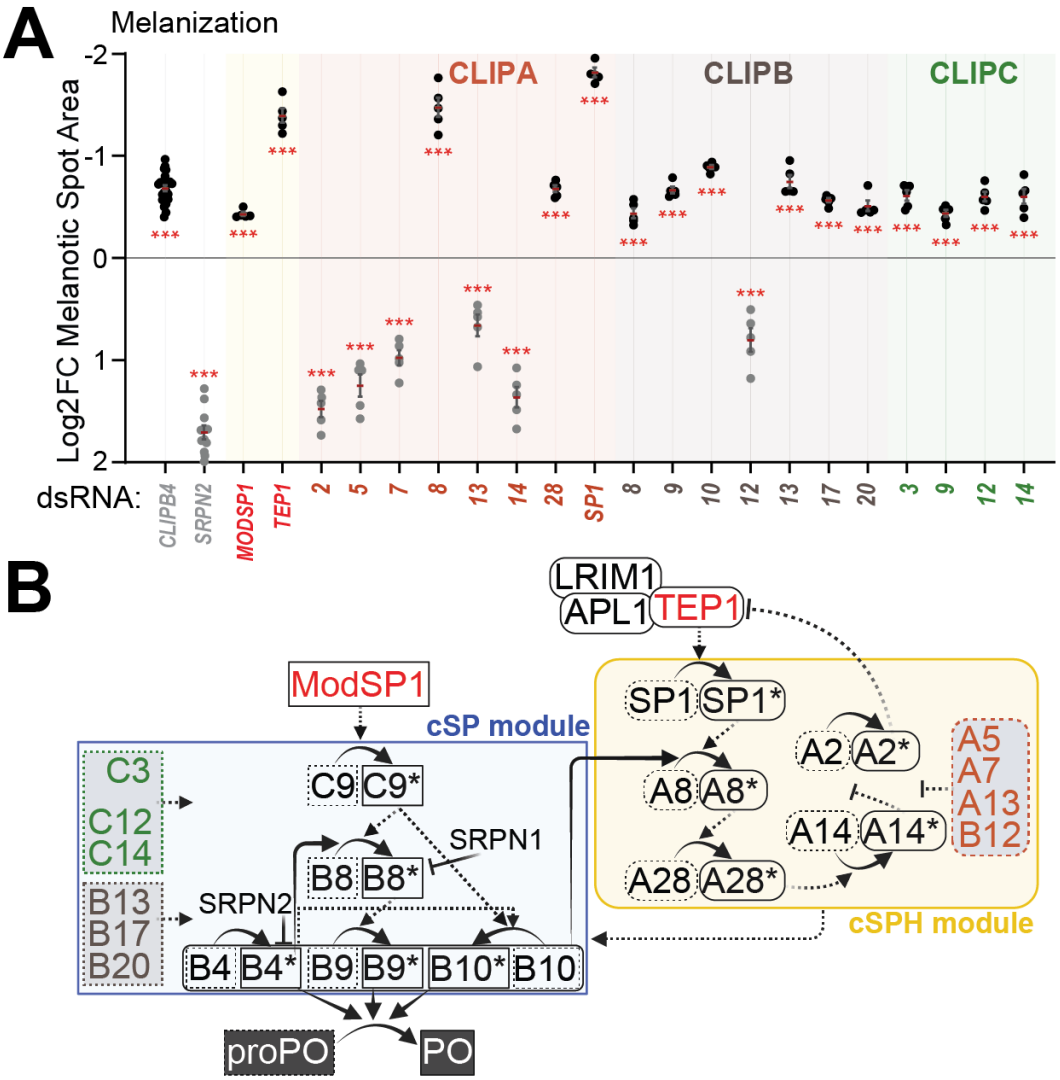

Fig. 2. An unprecedented number of CLIPs contribute to melanization in *Anopheles gambiae*. (**A**) MelASA RNAi screen identified 20 CLIPs, MODSP1 and TEP1 as regulators of melanization. Data shown as log2 fold change (FC) Total spot area relative to ds*GFP* injected mosquitoes challenged with lyophilized *M. luteus* suspension (n=50). Knockdown of *CLIPB4* and *SRPN2* were used as positive controls for positive and negative regulators, respectively. Red line and error bars represent mean ± SE from five biological replicates. One-way ANOVA followed by Bonferroni's post-tests were performed on ZOI data to calculate statistical significance (*** $P < 0.0001$). (**B**) Proposed model of the *An. gambiae* proPO activation cascades, including the interactions and hierarchies within and across the cSP (blue) and cSPH (yellow) modules. We identified 6 new cSPs that promote melanization (shown in green and brown), and 4 new cSPHs that inhibit melanization (shown in orange). Their placement within their respective modules is currently unknown. Dashed lines indicate interactions inferred from *in vivo* genetic studies. Solid lines indicate direct interactions inferred from *in vitro* biochemical assays. *Active cSP or cSPH. Arrows and lines with perpendicular bars indicate direction of positive and negative interactions, respectively.

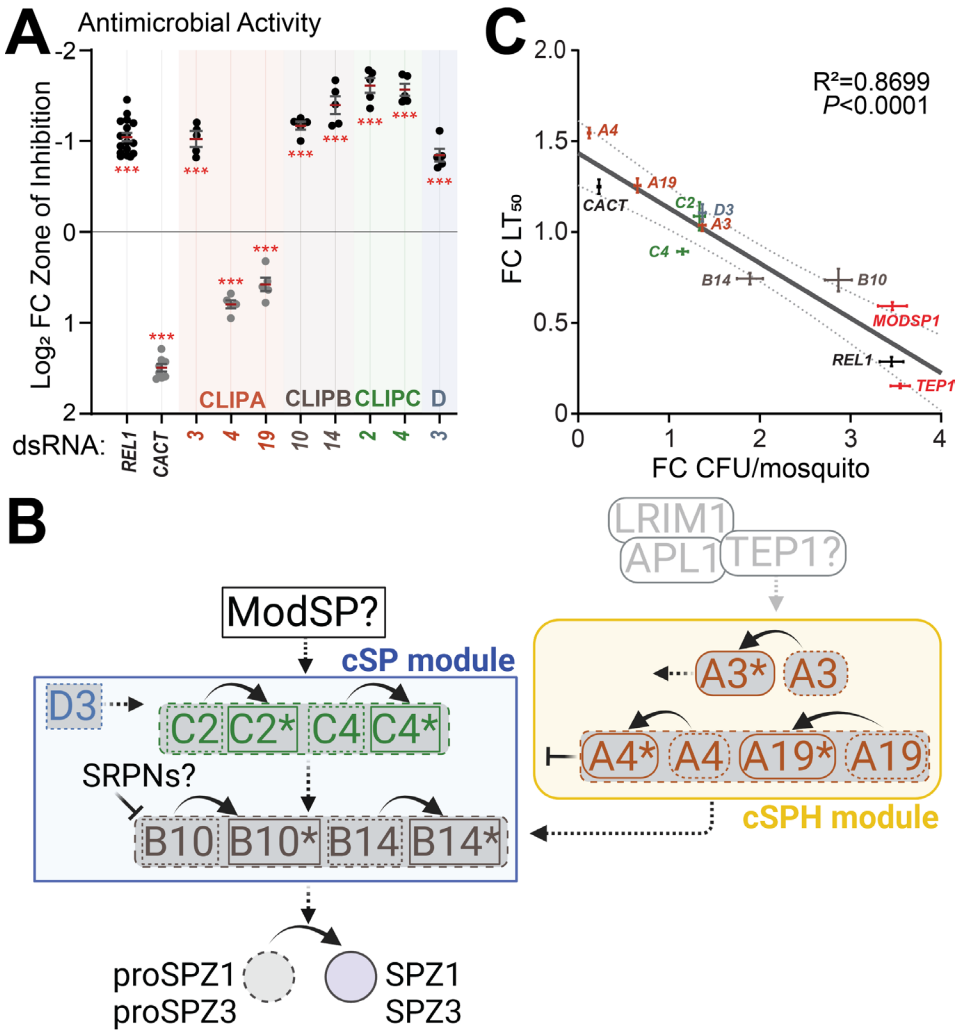

Fig. 3. A CLIPs cascade orchestrates antimicrobial defenses that are crucial for resistance to bacterial infection in *Anopheles gambiae*. (**A**) ZOI RNAi screen identified 8 CLIPs as regulators of antimicrobial activity. Data shown as log2 fold change (FC) ZOI relative to ds*GFP* injected mosquitoes challenged with *M. luteus* suspension (n=40). *REL1* and *CACT* kds were used as positive controls for positive and negative regulators, respectively. Red line and error bars represent mean ± SE from five biological replicates. One-way ANOVA followed by Bonferroni's post-tests were performed on ZOI data to calculate statistical significance (*** P < 0.0001). (**B**) Proposed model of the *An. gambiae* SPZ activation cascades, including hierarchies within and across the cSP (blue) and cSPH (yellow) modules. We identified 6 cSPs that promote, and 2 cSPHs that inhibit antimicrobial activity. *Active cSP or cSPH. (**C**) Higher bacterial load after silencing regulators of antimicrobial activity correlated with lower median survival. Data shown as mean log2 FC Colony Forming Units (CFU)/mosquito and Lethal Time 50 (LT_{50}) ± SE (n=5) plotted on linear x and y-axes, respectively. Solid line represents linear regression, dotted lines show 95% confidence bands. Pearson correlation coefficient= -0.9327.

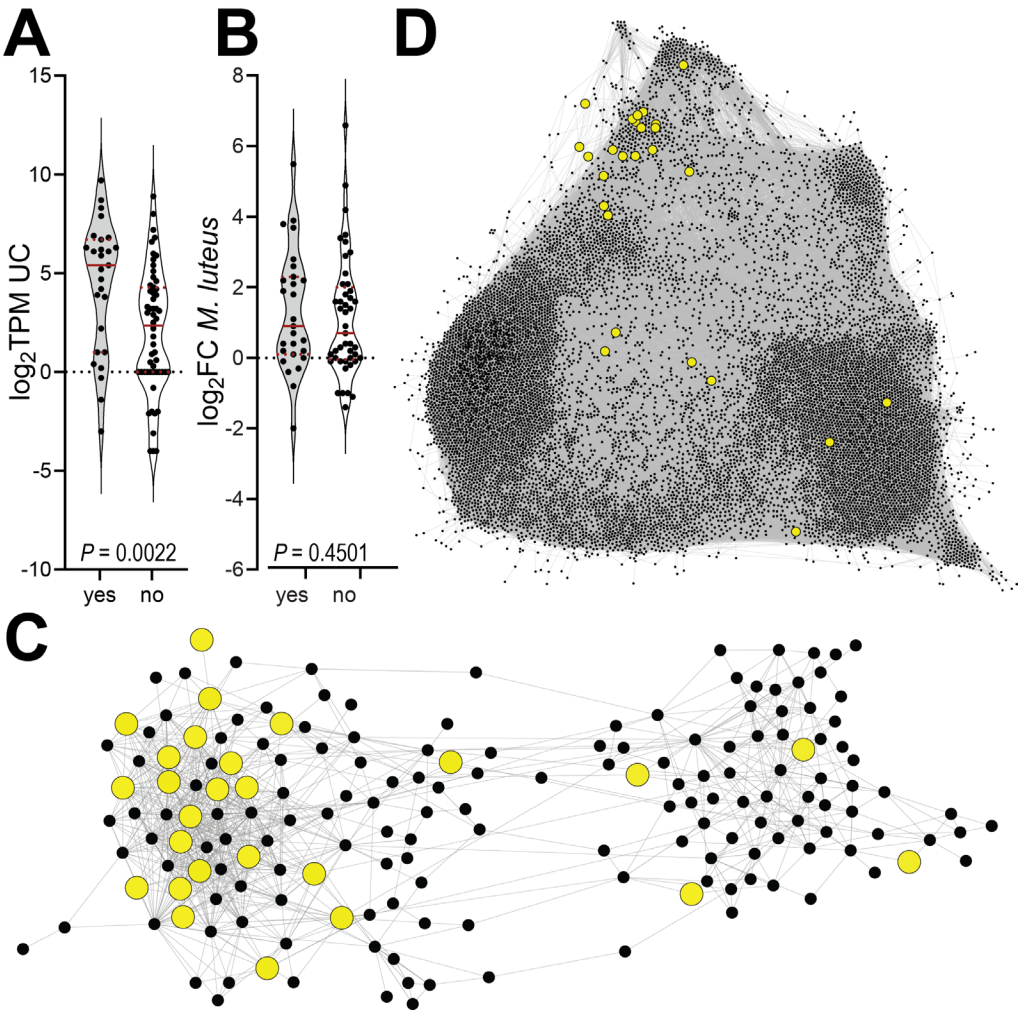

Fig. 4. Immunoregulatory CLIPs are globally co-expressed, but not regulated by infection. (**A**) Expression levels of immunoregulatory CLIPs (yes), as measured by log2 Transcripts per million (TPM), are significantly higher in naïve adult female mosquitoes as compared non-phenotypic CLIPs (no). (**B**) However, no difference is observed in fold change after *M. luteus* challenge between these two. Violin plots show the comparisons indicated in each panel, with red solid and dashed lines representing median and interquartile range limits, respectively. *P* values of unpaired two-tailed t-tests are shown in each panel. (**C,D**) The AgMelGCN2.0 (**C**) and the AgGCN1.0 networks (**D**). Positive and negative immunoregulatory CLIPs cluster mostly in one community of both networks, AgMelGCN (Community 2) and AgGCN1.0 (Community 7). Network images generated in Gephi 0.9.2 (Forceatlas 2, settings: Thread s number, 19; Tolerance, 1.0; approximate repulsion, checked; Scaling, 5.0; Gravity, 1.0; Prevent Overlap, checked; Edge Weight influence, 1.0)).